Computational Investigation of 5.5'',7''-trihydroxy-3,7-dimethoxy-4'-4'''-O-biflavone from Flavonoids Using DFT Calculations and Molecular Docking

Mehmet BAĞLAN[1,*], Ümit YILDIKO[2], Kenan GÖREN[1]

[1]Kafkas University, Department of Chemistry, Kars 36100, Türkiye
mehmetbaglan36@gmail.com , ORCID:0000-0002-7089-7111
kenangoren49@gmail.com , ORCID:0000-0001-5068-1762
[2]Kafkas University, Department of Bioengineering, Kars 36100, Türkiye
yildiko1@gmail.com , ORCID:0000-0001-8627-9038

Abstract

The structural characterization of the 5.5'',7''-trihydroxy-3,7-dimethoxy-4'-4'''-*O*-biflavone (TDOB) molecule was done in this study. For the structural characterization of this molecule, based on the molecule's stable phase geometry, entire calculations were done using the CAM-B3LYP and PBEPBE approaches with SDD and LanL2DZ basis sets respectively. In our study, many calculations, such as HOMO-LUMO energy gaps, inter-orbital, and inter-orbital bond interactions, and electrostatic surface mapping processes of the TDOB molecule, have also been made. In the continuation of our study, the specific binding site and mechanism of the ligand on the protein were investigated using molecular docking. In the molecular docking study, affinity scores for TDOB- aldose reductase (PDB: 4ICC) and (PDB: 4IGS) were found to be -8.559 kcal/mol and -5.461 kcal/mol, respectively. The 4ICC receptor binding score was found to be greater. In the continuation of the molecular docking study, the inhibitory properties of TDOB were investigated against the aldose reductase enzymes (PDB: 4ICC) and (PDB: 4IGS), both of which showed effective inhibition, and it was seen that the TDOB molecule effectively inhibited the enzymes (PDB: 4ICC) and aldose reductase (PDB: 4IGS).

Keywords: Flavonoids; TDOB; HOMO-LUMO; Molecular docking.

5,5'',7''-trihidroksi-3,7-dimetoksi-4'-4'''-O-biflavon Bileşiğinde DFT ve Moleküler Doking Çalışması

Öz

Bu çalışmada, 5,5'',7''-trihidroksi-3,7-dimetoksi-4'-4'''-*O*-biflavon (TDOB) molekülünün yapısal karakterizasyonu yapıldı. Bu molekülün yapısal karakterizasyonu için, molekülün kararlı faz geometrisine dayalı olarak, tüm hesaplamalar sırasıyla CAM-B3LYP ve PBEPBE metotlarını SDD ve LanL2DZ temel seti kullanılarak yapıldı. Çalışmamızda TDOB molekülünün HOMO-LUMO enerji boşlukları, yörüngeler arası ve yörüngeler arası bağ etkileşimleri, elektrostatik yüzey haritalama işlemleri gibi birçok hesaplamalarda yapılmıştır. Çalışmamızın devamında moleküler doking kullanılarak ligandın protein üzerindeki spesifik bağlanma yeri ve mekanizması araştırıldı. Doking çalışmasında, TDOB- aldoz redüktaz (PDB: 4ICC) ve TDOB- aldoz redüktaz (PDB: 4IGS) ile afinite skorları sırasıyla -8.559 kcal/mol ve -5.461 kcal/mol olarak bulundu. TDOB- aldoz redüktaz (PDB: 4ICC) reseptör bağlanma skoru daha büyük olduğu tespit edildi. Moleküler doking çalışmasının devamında TDOB'nin inhibitör özellikleri, her ikisi de etkili inhibisyon gösteren (PDB: 4ICC) ve (PDB: 4IGS) enzimlerine karşı araştırıldı ve TDOB molekülünün, (PDB: 4ICC) ve (PDB: 4IGS) aldoz redüktaz enzimlerini etkili bir şekilde inhibe ettiği görüldü.

Anahtar Kelimeler: Flavonoidler; TDOB; HOMO-LUMO; Moleküler doking.

1. Introduction

Flavonoids are natural substances that belong to a group of plant secondary metabolites with a polyphenolic structure found in vegetables, fruits, and certain beverages [1]. Flavonoids have biochemical and antioxidant capabilities that have been linked to diseases like Alzheimer's, atherosclerosis, and cancer [2, 3]. Flavonoids play a key role in a wide array of nutraceutical, pharmacological, medicinal, and cosmetic areas owing to their numerous health-promoting properties [4, 5]. Their antioxidant, anti-carcinogenic, anti-inflammatory, and anti-mutagenic qualities, with their potential to alter critical cellular enzyme activity, contribute to this [6]. Potent inhibitors of flavonoids include xanthine oxidase (XO), lipoxygenase, cyclo-oxygenase (COX), and phosphoinositide 3-kinase [7]. Flavonoids are plant-derived substances found in various plant parts. Flavonoids are essential for the growth of vegetables and protect themselves from plaque, so they are also known as low-molecular-weight phenolic compounds found in plants. Because flavonoids are one of the most recognized chemical groups in high plants, they are easily recognized as floral pigments found in most angiosperm groups [8, 9]. Yet they are not only found in flowers; they are also found in other plants like chalcones, flavones, flavonols, and isoflavones.

Computational chemistry has made significant progress as a tool to study organic and biological structures, especially in various fields of chemistry [10]. Theoretical chemical calculations have proven crucial in elucidating the molecule's architectures, properties, processes, and reaction selectivity. The most common theoretical approaches used to calculate various molecular properties include DFT (density functional theory), optimized molecular structures, vibrational frequencies, and chemical shifts [11-13].

The CAM-B3LYP/SDD and PBEPBE/LanL2DZ level of theory was used to investigate the theoretical spectroscopic features of the TDOB molecule in this research. The study was then subjected to molecular docking to determine the ligand's specific binding location over the protein as well as the binding's mechanism. Following the selection of the optimal pose for the entire ligand-enzyme docking, binding modalities were studied in order to better understand inhibitory mechanisms.

2. Materials and Methods

Entire calculations were made in Gaussian 09 software [14] by use of CAM-B3LYP/SDD and PBEPBE/LanL2DZ level of theory of DFT calculations. The first step in the computational analysis was to optimize the geometry of the generated molecule. The TDOB molecule, in particular, requires low energy sensitivity to molecular shape changes caused by core position displacement. Especially for TDOB, low energy sensitivity to changes in molecular structure is required due to core position displacement. Gaussian 09's DFT method was used to calculate the molecular structure, vibrational frequencies, and energies of optimal geometries of the TDOB molecule. The basic set is the Lee's-Yang-Parr correlation function (CAM-B3LYP) based on the SDD-based program package.

Molecular docking was done to look at the specific binding site and the ligand's mechanism over the protein (using the Maestro Molecular Modeling platform (version 11.8) of the Schrödinger, LLC model) [15]. High-resolution (0.85 Å) crystal structures were obtained from the enzymes aldose reductase (PDB: 4ICC) and aldose reductase (PDB: 4IGS) (https://www.rcsb.org/structure/4IGS/pdb). Ligand constructs were obtained as SDF files from the PubChem website. All compounds were synthesized according to the previous implementation of the Ligprep module [16, 17]. Using the wizard module, protein preparation was put on hold for data. At this point, all water molecules have been expelled from the crystal structure [18]. The protein ion balance was once again adjusted using this module, this time by identifying the active site of the protein for flexible binding. Mesh boxes were created as the basis of the receptor griding module and formed networks at the protein's binding sites, allowing

flexible docking. These studies followed the same procedures as previous studies. The slip insertion module was used to construct a ligand-protein docking strategy [19]. Optimal binding energies were calculated based on interactions between ligand and protein, π-π interactions, hydrogen bonds, and alkyl and π interactions. Maximum binding affinity is indicated by the lowest energy configurations. Discovery Studio 4.5 was used to demonstrate the 2D and 3D interactions as well as the resulting receptor model [20].

3. Results and Discussion

3.1. Structure details and analysis

The optimal structural parameters estimated using the DFT/CAM-B3LYP/SDD and PBEPBE/LanL2DZ level of theory are given in [21, 22] Table 1. The two methods and base sets were used to compare the bond lengths and angles between the optimized molecule atoms. The bond lengths between C - O atoms in the molecule were calculated as 1.395 Å in the CAM-B3LYP level of theory and 1.410 Å in the PBEPBE level of theory when compared with the two techniques. In the second procedure, the bond lengths were shorter. In aromatic and aliphatic structures, bond lengths can be used with both approaches. Due to the sensitivity of the procedures, there are slight differences between them. Both methods are compatible at Fig. 1.

Table 1: The bond lengths (Å) or bond angles (o) of the TDOB molecule calculated theoretically

Bond Lengths	CAM-B3LYP/SDD	PBEPBE/LanL2DZ	Bond Lengths	CAM-B3LYP/SDD	PBEPBE/LanL2DZ
C1-C2	1.399	1.412	C2-O8	1.395	1.410
C5-C7	1.472	1.473	C16-O15	1.391	1.404
C13-C14	1.397	1.406	C18-O26	1.276	1.304
C18-C19	1.449	1.450	C23-O25	1.361	1.372
C31-C32	1.462	1.467	C32-O60	1.385	1.397
C33-C34	1.405	1.419	O8-C9	1.400	1.417
C34-O39	1.376	1.394	O39-C40	1.449	1.469
C1-H41	1.083	1.093	O25-H53	1.006	1.045
C20-H50	1.081	1.090	O37-C56	1.004	1.041
C40-H57	1.089	1.106	O60-C61	1.466	1.488
Bond Angles	**CAM-B3LYP/SDD**	**PBEPBE/LanL2DZ**	**Bond Angles**	**CAM-B3LYP/SDD**	**PBEPBE/LanL2DZ**
C1-C2-C3	120.622	120.599	C21-C22-H51	122.013	121.928
C4-C5-C7	121.070	121.003	C21-O24-H52	113.194	111.159
C5-C7-C19	126.843	126.934	C7-O15-C16	121.135	120.175
C17-C18-O26	121.313	121.019	C34-O39-C40	119.379	118.057
C23-O25-H53	109.718	106.749	H57-C40-H59	109.760	109.891
Bond Angles	**CAM-B3LYP/SDD**	**PBEPBE/LanL2DZ**	**Bond Angles**	**CAM-B3LYP/SDD**	**PBEPBE/LanL2DZ**
C18-C17-C16-C20	-179.945	-179.921	C35-C36-O37-H56	179.243	178.928

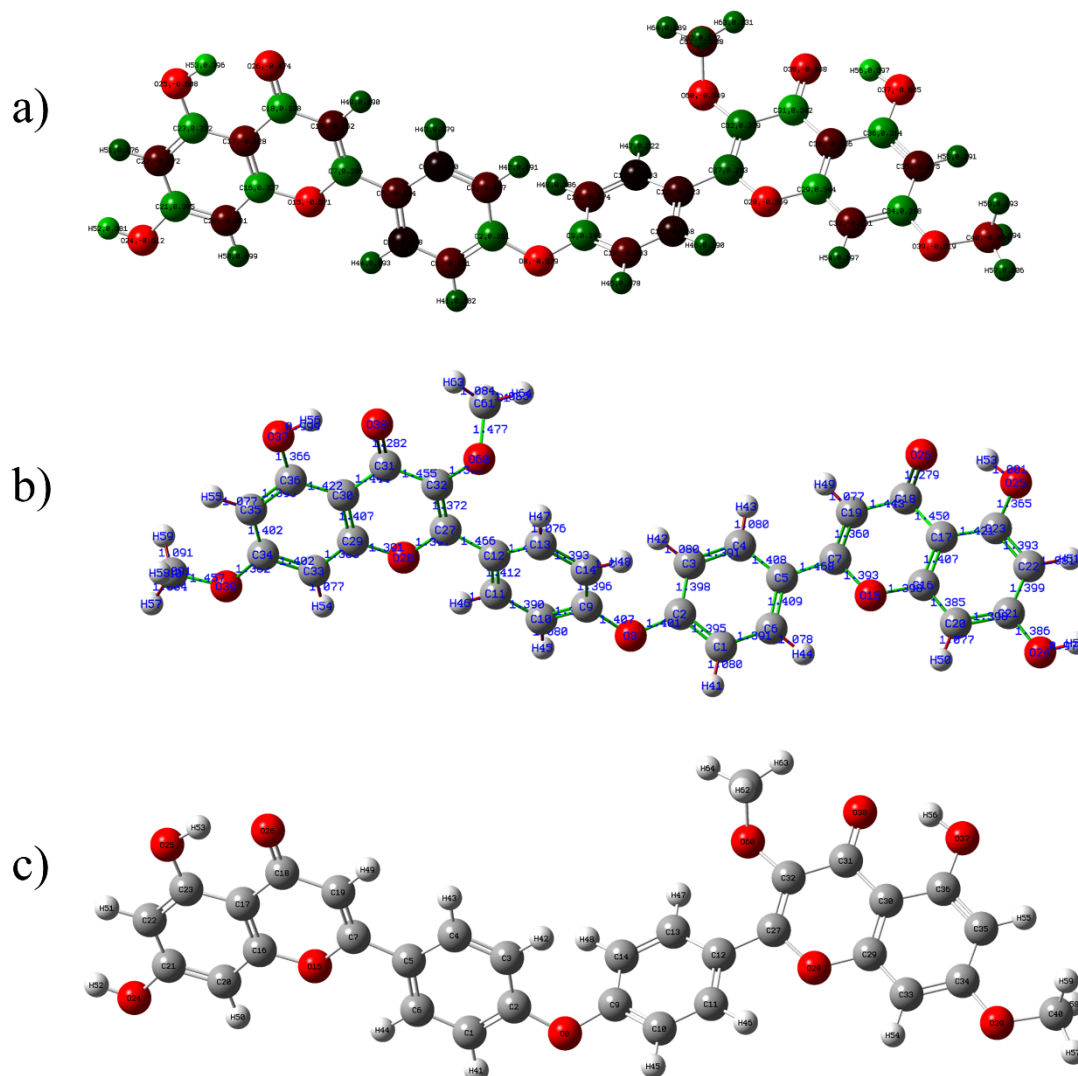| C11-C12-C27-C32 | -164.920 | -166.661 | O28-C27-C32-O60 | 177.309 | 176.626 |
| C21-C22-C23- O25 | 179.981 | 179.946 | C12-C27-O28-C29 | -179.856 | -178.716 |

Figure 1: TDOB molecule with CAM-B3LYP/SDD level of theory a) Mulliken b) bond length c) structure optimization

3.2. Frontier molecular orbitals (FMOs)

The highest and occupied molecular orbitals (HOMOs) or the lowest and unoccupied molecular orbitals (LUMOs) are two types of frontier molecular orbitals [23, 24]. Apart from chemical interactions, FMOs have a key role in UV-Vis spectra, as well as electrical and optical properties [25]. The electron-donating ability of an inhibitor molecule is often linked to HOMO, according to the boundary orbital theory. The electron-donating ability of a molecule has been proven by high E_{HOMO} values. The electron-accepting ability of molecules has been proven by

ELUMO. TDOB molecule's CAM-B3LYP/SDD and PBEPBE/LanL2DZ level of theory and HOMO and LUMO boundary trajectories are shown in Fig. 2 and Fig. 3. While the E_{HOMO} = -7.5 eV-E_{LUMO} = -1.40 eV of the molecule was calculated by the DFT/CAM-B3LYP/SDD level of theory, the E_{HOMO} = -7.5 eV-E_{LUMO} = -1.41 eV of the DFT/ PBEPBE/ LanL2DZ level of theory was calculated. For other orbitals, E_{HOMO-1} = -7.8 eV-E_{LUMO+1} = -1.22 eV was calculated for the DFT/CAM-B3LYP/SDD level of theory, and E_{HOMO-1} = -7.8 eV-E_{LUMO+1} = -1.23 eV for DFT/ PBEPBE/LanL2DZ level of theory values were calculated. The HOMO and LUMO orbitals of the molecule determine how it will interact with other molecules. The energy band gap (E = ELUMO – EHOMO) has low absolute values indicating limited high chemical reactivity and kinetic stability [26]. The band gaps of the compound in both methods are high around 6.00 eV, indicating that it is an insulating material. The electronegativity of a small orbital gap indicates a molecule with polarization, stiffness, and other reactivated indices [27]. Chemical reactivity indices are shown in Table 2.
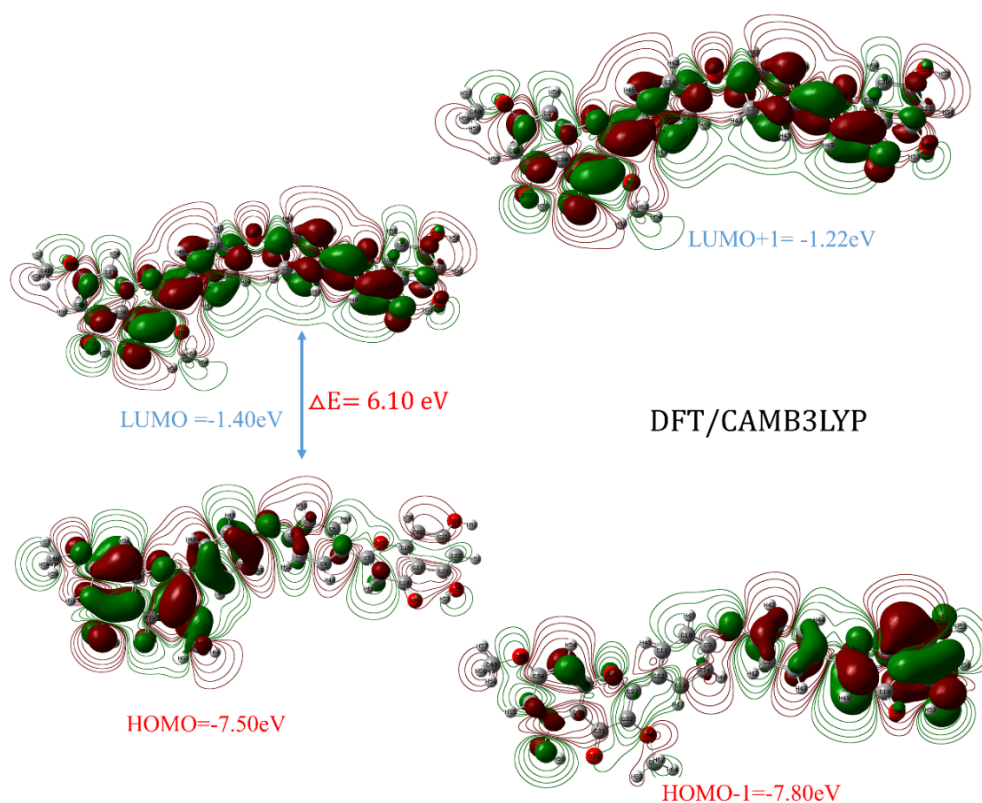

Figure 2: According to the DFT /CAM-B3LYP/SDD level of theory, the compound's boundary molecular orbitals
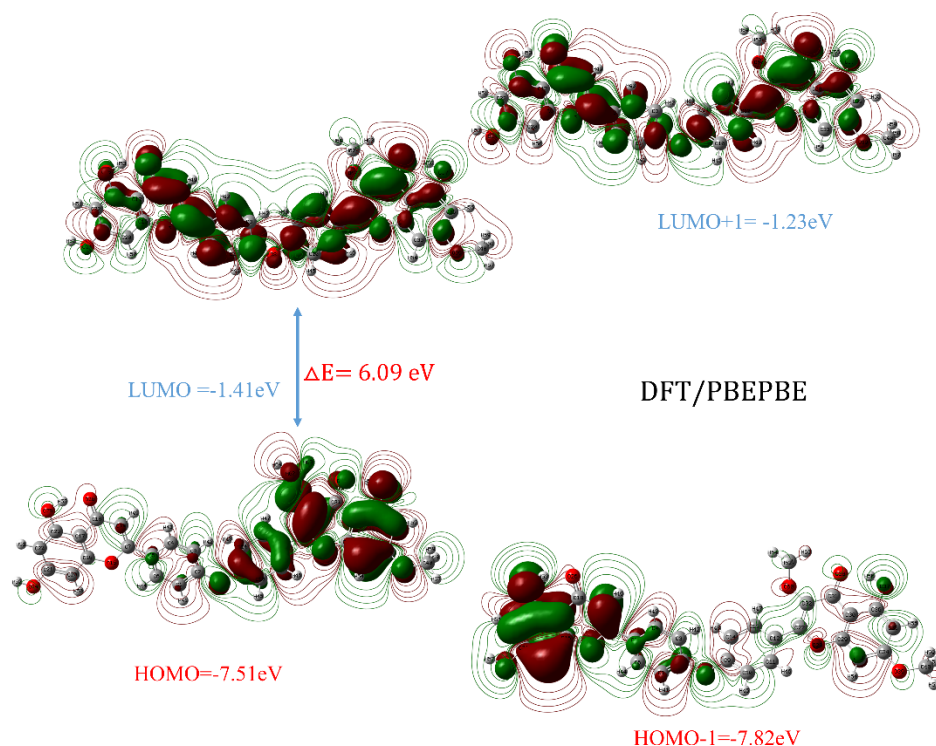
LUMO+1= -1.23eV

LUMO =-1.41eV

$\Delta E= 6.09$ eV

DFT/PBEPBE

HOMO=-7.51eV

HOMO-1=-7.82eV

Figure 3: According to the DFT/PBEPBE/LanL2DZ level of theory, the compound's boundary molecular orbitals

Table 2: Calculation using DFT/CAM-B3LYP/SDD- DFT/PBEPBE/LanL2DZ level of theory to compare HOMO, LUMO, and chemical reactivity descriptors at 298.15 K in the base case

Molecules Energy	DFT/CAM-B3LYP	DFT/ PBEPBE
E_{LUMO}	-1.40	-1.41
E_{HOMO}	-7.50	-7.51
E_{LUMO+1}	-1.22	-1.23
E_{HOMO-1}	-7.80	-7.82
Energy Gap (Δ) $|E_{HOMO}- E_{LUMO}|$	6.10	6.09
Ionization Potential ($I = -E_{HOMO}$)	7.50	7.51
Electron Affinity ($A = -E_{LUMO}$)	1.40	1.41
Chemical hardness ($\eta = (I - A)/2$)	3.05	3.05
Chemical softness ($s = 1/2\ \eta$)	0.164	0.164
Chemical Potential ($\mu = -(I + A)/2$)	-4.45	-4.46
Electronegativity ($\chi = (1 + A)/2$)	1.2	1.21
Electrophilicity index ($\omega = \mu^2/2\ \eta$)	3.24	3.26

3.3. Non-linear optical properties (NLO)

Non-linear optical (NLO) materials having two substantial absorptions have sparked a lot of interest in recent years. Two-photon absorption' behavior can be influenced by factors like molecular weight, molecule symmetry, and solubility. In addition, The dipole moment provides a strong intermolecular attraction, containing dipole-dipole and van der Waals-type interactions, as well as a substantial characteristic of the energy associated with the electric field applied within

the molecule [28, 29]. Table 3 lists the calculated parameters for the electronic dipole moment and total dipole moment. In the gas phase, parameters for the CAM-B3LYP/SDD level of theory $\mu = 3.4723$ D, $\alpha = 240.6017$ au, $\beta = 1.699 \times 10^{-31}$ esu, and for the PBEPBE/LanL2DZ level of theory $\mu = 4.7335$ D, $\alpha = 230.5635$ au, $\beta = 2.316 \times 10^{-31}$ was calculated as esu. From the data obtained for this molecule, theoretically high polarity values are considered to be good candidates for nonlinear optical materials [30].

Table 3: Polarizability (au), dipole moments (Debye), β sum, and β components of C-O value calculated with DFT/CAM-B3LYP/SDD and DFT/PBEPBE/LanL2DZ level of theory

Parameters	CAM-B3LYP/ SDD	PBEPBE/ LanL2DZ	Parameters	CAM-B3LYP/ SDD	PBEPBE/ LanL2DZ
μ_X	2.7749	2.4388	β_{XXX}	251.8406	261.7705
μ_Y	-2.0722	-3.0020	β_{YYY}	-58.2712	-53.0664
μ_Z	0.2505	0.6656	β_{ZZZ}	0.1694	0.1664
$\mu_{(D)}$	3.4723	4.7335	β_{XYY}	59.0378	60.5733
α_{XX}	-204.7813	-203.6619	β_{XXY}	-68.2085	-67.1160
α_{YY}	-268.1013	-267.7645	β_{XXZ}	1.1489	1.3641
α_{ZZ}	-243.3164	-247.2643	β_{XZZ}	19.5879	18.4797
A_{XY}	8.2697	7.6678	β_{YZZ}	17.0889	16.9470
α_{XZ}	18.9743	18.4972	β_{YYZ}	-14.1439	-12.2315
α_{YZ}	-2.5606	-2.4441	β_{XYZ}	5.7929	8.0334
α (au)	240.6017	230.5635	β (esu)	1.699×10^{-31}	2.316×10^{-31}

3.4. Mulliken atomic charges

The application of quantum chemistry computations relies heavily on Mulliken atomic charge estimates. Mulliken can be used to get many ideas about atomic charge polarization, stability, electronic structure, etc [31]. It also shows how to charge sharing and molecular charge transfer help build electron donor-acceptor pairs. The CAM-B3LYP/SDD level of theory was used to calculate the Mulliken atom. The oxygen atom linked to the aromatic ring has a Mulliken charge of O24 (-0.458) - (-0.425), O26 (-0.359) - (-0.343), O38 (-0.377) - (-0.369), and O60 (-0.355) - (-0.314). Some C atoms were found to be positive, while others were found to be negative. Mulliken atomic charge calculation has an important role for the application of quantum chemical calculation of molecular system. Atomic charge affects the dipole moment, polarizability, electronic structure and other molecular properties of the system [32].

Table 4: Values found using DFT/CAM-B3LYP/SDD and DFT/PBEPBE/LanL2DZ level of theory to determine Mulliken atomic charges for TDOB molecule

	CAM-B3LYP/ SDD	PBEPBE/ LanL2DZ		CAM-B3LYP/ SDD	PBEPBE/ LanL2DZ
C1	-0.372	-0.383	O24	-0.458	-0.425
C2	0.334	0.328	O25	-0.454	-0.489
C4	-0.347	-0.368	O26	-0.359	-0.343

C7	0.275	0.225	**O28**	-0.333	-0.294
C9	0.330	0.324	**O38**	-0.377	-0.369
C13	-0.344	-0.362	**O39**	-0.299	-0.256
C19	-0.439	-0.402	**O60**	-0.355	-0.314
C22	-0.566	-0.572	**H41**	0.268	0.265
C27	0.162	0.111	**H43**	0.236	0.234
C29	0.323	0.266	**H46**	0.276	0.271
C30	-0.071	0.021	**H47**	0.313	0.303
C32	0.094	0.124	**H48**	0.271	0.271
C34	0.439	0.388	**H51**	0.259	0.254
C35	-0.533	-0.354	**H53**	0.412	0.383
C36	0.213	0.186	**H54**	0.293	0.283
C40	-0.475	-0.544	**H62**	0.199	0.219

3.5. Molecular electrostatic potential (MEP)

The molecular electrostatic potential (MEP) is plotted for the TDOB molecule and shows the molecule's shape, size, and electrostatic potential values. The investigation of the molecular structure's physicochemical properties has been substantially aided by molecular electrostatic potential (MEP) mapping [33, 34]. A portion of the molecule with a negative electrostatic potential is vulnerable to electrophilic assault. Different electrostatic potential levels on the surface are reflected in the changing colors; yellow and red indicate the highest negative zone, which is the preferred region for electrophilic reagents. The maximum positive range, which is the preferred range of nucleophilic reactivity, is expressed by the zero potential as shown in the blue and green regions. Here, the TDOB molecule's MEP map is mapped as shown in Fig. 4. The aromatic ring area appears to be neutral (green) in coloring.
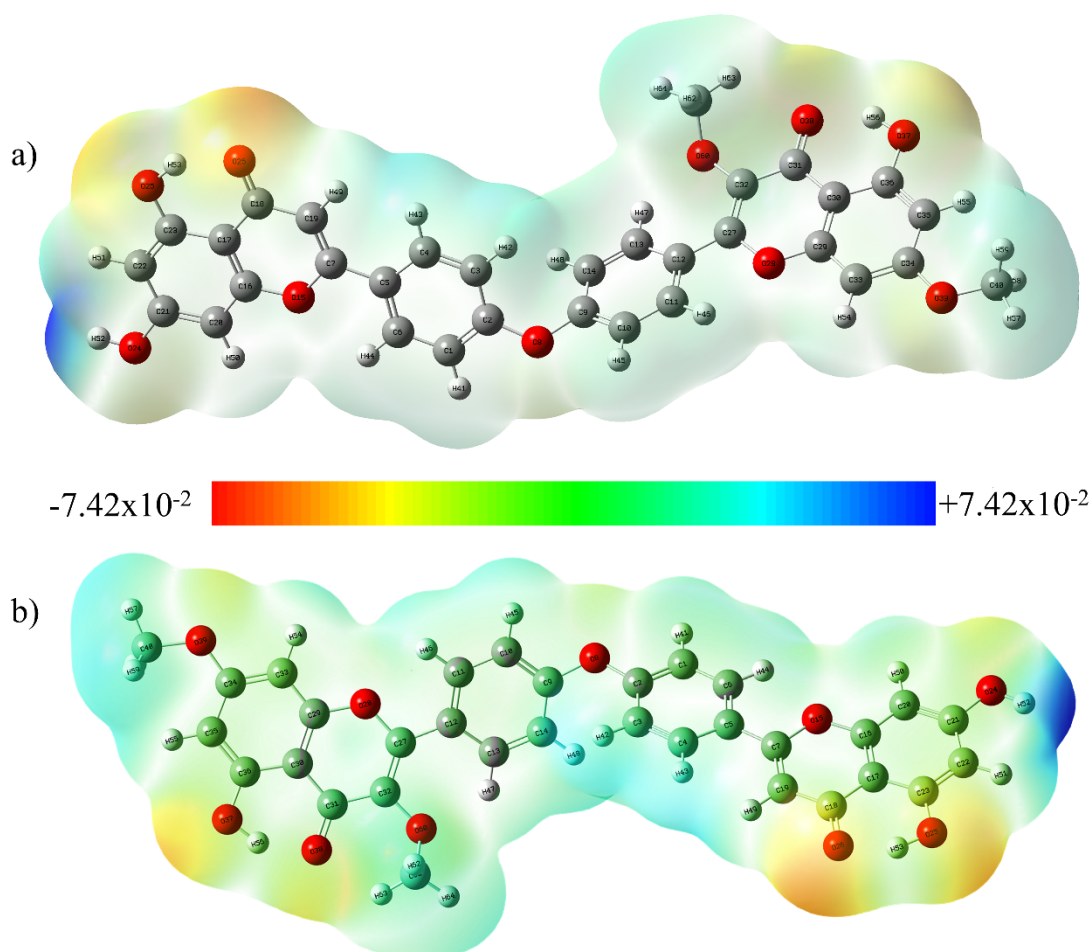
Figure 4: Molecular electrostatic potential surface calculated using the DFT/CAM-B3LYP/SDD **(a)** and PBEPBE/LanL2DZ **(b)** level of theory

3.6. Molecular docking studies

Molecular docking is a computer method that aims to forecast the non-covalent interaction between a macromolecule (receptor) and a small molecule (ligands). Automated docking is frequently used in structure/function analysis and molecular design for the prediction of bimolecular complexes. The structure-based drug design process includes steps such as docking small molecule compounds into a receptor's binding site and determining the complex's binding affinity [27, 35]. As a result of the TDOB - aldose reductase (PDB: 4ICC) docking study, Fig. 5 shows the 3D and 2D interaction. The shift score in binding affinity with TDOB - aldose reductase (PDB: 4ICC) was found to be -8.559 kcal/mol (Table 5). The binding mechanism is here, in the TRP-112 (5.49 Å) phenol binding mechanism with hydrogen-bonded water, ILE-261 (4.69 Å) hydrogen bonded to phenol, ILE-261 (3.65 Å), SER-211 (4.03 Å), ASP-44 (3.63 Å), THR-20 (5.30 Å), conventional hydrogen bond, GLY-19 (3.66 Å) conventional hydrogen bond attached to hydrogen in hydroxyl, SER-215 (3.40 Å) hydrogen bond attached to carbon, CYS-299 (7.41

Å) alkyl attached to the middle of the benzene ring, TYR-210 (5.69 Å), TRP-21 (5.09 Å) and TRP-21 (5.65 Å) π -alkyl attached to the core of the benzene are examples. Figure 5 shows additional interactions. Figure 5 depicts a 3D view of the SAS surface on the receptor.

Table 5: Docking score of TDOB - aldose reductase (PDB: 4ICC) and TDOB - aldose reductase (PDB:4IGS)

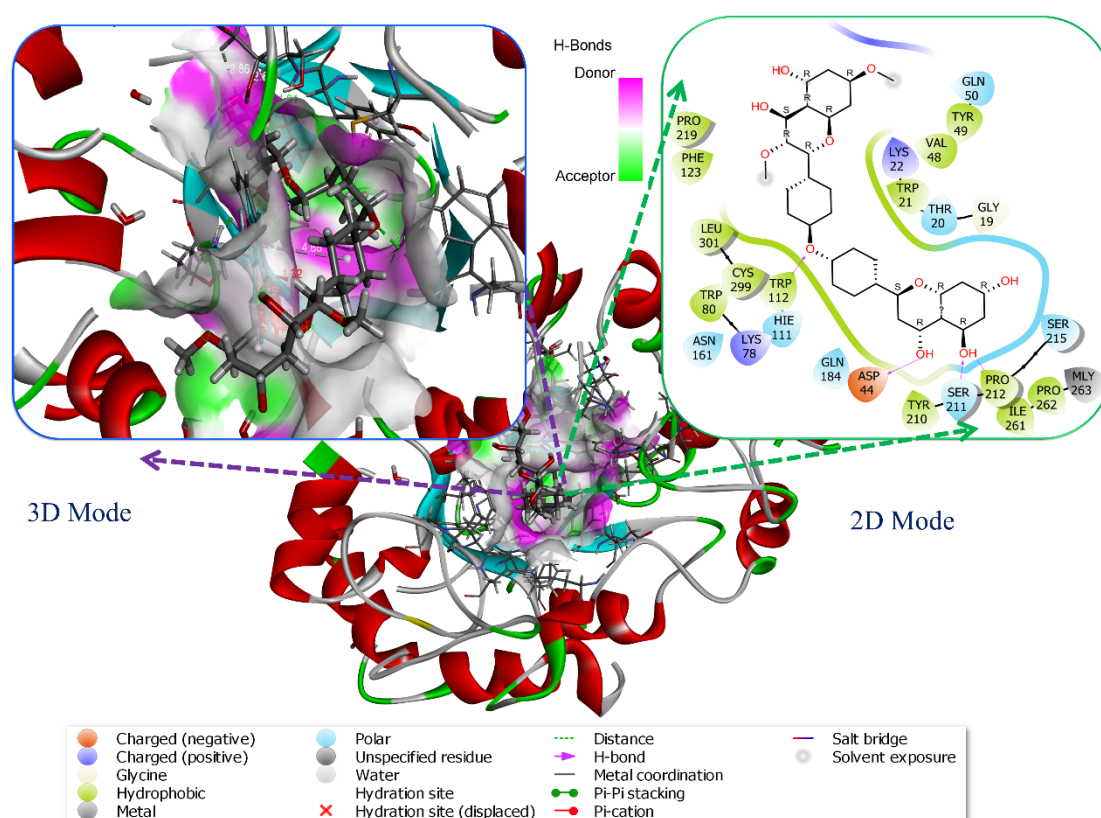| Compound	Docking Score	
	Aldose reductase (PDB:4ICC)	Aldose reductase (PDB:4IGS)
TDOB	-8.559 kcal/mol	-5.461 kcal/mol

Figure 5: 2D picture of TDOB - aldose reductase (PDB: 4ICC) enzyme interactions and 3D view of the receptor's aromatic surface

As a result of AKR1B1 (PDB:4IGS) docking, the 3D and 2D interactions are shown in Fig. 6. The shift score in binding affinity with TDOB - aldose reductase (PDB:4IGS) was found as -5.461 kcal/mol (Table 5). The binding mechanism is here, PRO-225 (4.41 Å), ARG-217 (5.55 Å), GLU-229 (5.63 Å), ASP-216 (3.37 Å) conventional hydrogen bonding in hydroxyl, ASP-216

(4.63 Å) and ASP-216 (3.31 Å) carbon hydrogen bonds, ALA-220 (4.72 Å), ALA-220 (4.90 Å), PRO-222 (4.57 Å), and PRO-218 (5.17 Å) are examples of alkyl bonded to the middle of the benzene ring. Figure 6 shows other interactions. Figure 6 depicts a 3D view of the SAS surface on the receptor.
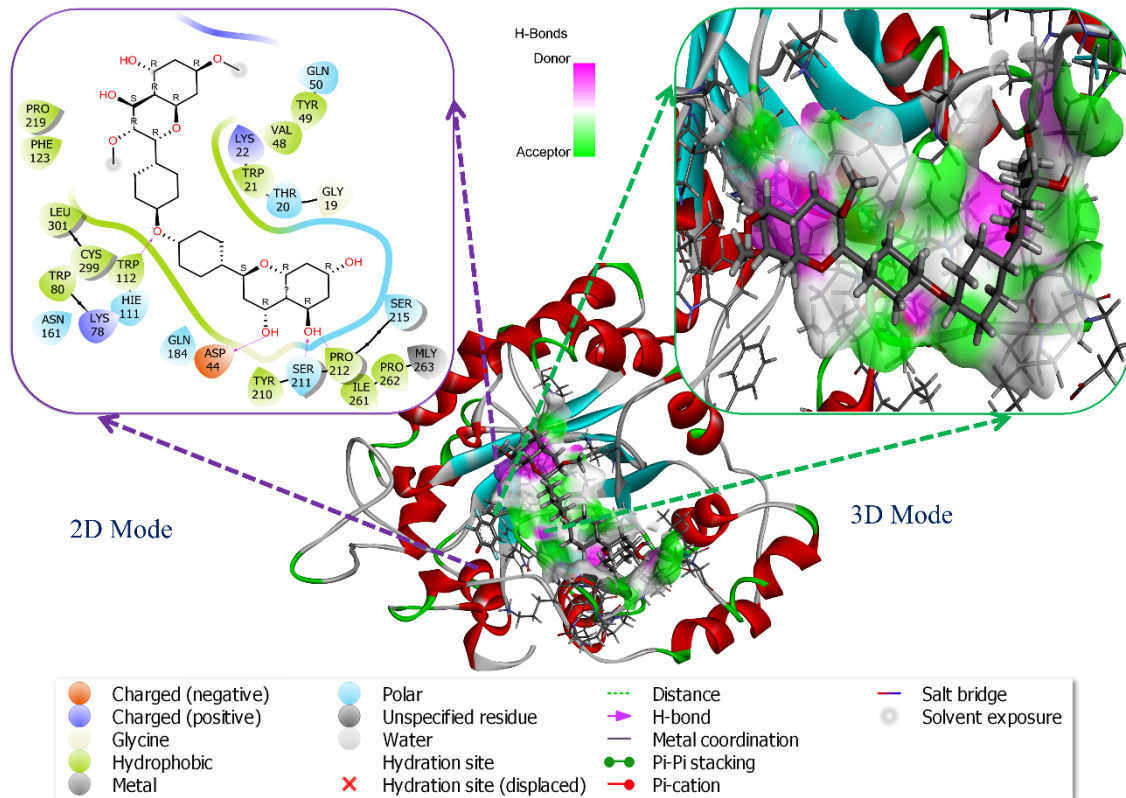

Figure 6: 2D picture of TDOB - aldose reductase (PDB: 4IGS) enzyme interactions and 3D view of the receptor's aromatic surface

4. Conclusion

Quantum chemical calculations were used to make detailed studies on TDOB molecule. The structural, electronic, and vibrational frequencies of the compound were estimated using the CAM-B3LYP/SDD and PBEPBE/LanL2DZ levels of theory. The compound's bond angles, bond lengths, and dihedral angles were theoretically defined structural parameters. The compound's Nonlinear optical properties were also examined. It was also determined that the studied compound could be used as an NLO material. HOMO-LUMO, MEP maps, and Mulliken atomic charges are also depicted. TDOB molecule's molecular docking was also done to look at the specific binding site and mechanism of the ligand on the protein. After finding the optimal exposure for all ligand-enzyme docking, binding modalities were studied to better understand inhibitory mechanisms. In the study, the shift scores in binding affinity with TDOB– aldose

reductase (PDB: 4ICC) and TDOB– aldose reductase (PDB: 4IGS) were determined to be -8.559 kcal/mol and -5.461 kcal/mol, respectively. It is more effective with TDOB – aldose reductase (PDB: 4ICC) receptor binding score. Since this compound has a high drug potential, it can be investigated in the design of new drugs in the treatment of Alzheimer's disease and as a new enzyme inhibitor candidate.

References

[1] Panche, A.N., Diwan, A.D., and Chandra, S.R., *Flavonoids: an overview,* Journal of Nutritional Science, 5 (47), 1-15, 2016.

[2] Oyeleke, M.B. and Owoyele, B.V., *Saponins and flavonoids from Bacopa floribunda plant extract exhibit antioxidant and anti-inflammatory effects on amyloid beta 1-42-induced Alzheimer's disease in BALB/c mice,* Journal of Ethnopharmacology, 288, 114997, 2022.

[3] Chauhan, B.S., Kumar, R., Kumar, P., Kumar, P., Sinha, S., Mishra, S.K., Kumar, P., Tiwari, K.N., Critchley, A.T., Prithiviraj, B., and Srikrishna, S., *Neuroprotective potential of flavonoid rich Ascophyllum nodosum (FRAN) fraction from the brown seaweed on an Aβ(42) induced Alzheimer's model of Drosophila,* Phytomedicine, 95, 153872, 2022.

[4] Wang, B., Ding, Y., Zhao, P., Li, W., Li, M., Zhu, J., and Ye, S., *Systems pharmacology-based drug discovery and active mechanism of natural products for coronavirus pneumonia (COVID-19): An example using flavonoids,* Computers in Biology and Medicine, 143, 105241, 2022.

[5] Mitra, S., Lami, M.S., Uddin, T.M., Das, R., Islam, F., Anjum, J., Hossain, M.J., and Emran, T.B., *Prospective multifunctional roles and pharmacological potential of dietary flavonoid narirutin,* Biomedicine and Pharmacotherapy, 150, 112932, 2022.

[6] Heimfarth, L., Nascimento, L.D.S., Amazonas da Silva, M.J., Lucca Junior, W., Lima, E.S., Quintans-Junior, L.J., and Veiga-Junior, V.F.D., *Neuroprotective and anti-inflammatory effect of pectolinarigenin, a flavonoid from Amazonian Aegiphila integrifolia (Jacq.), against lipopolysaccharide-induced inflammation in astrocytes via NFκB and MAPK pathways,* Food and Chemical Toxicology, 157, 112538, 2021.

[7] Onishi, S., Nishi, K., Yasunaga, S., Muranaka, A., Maeyama, K., Kadota, A., and Sugahara, T., *Nobiletin, a polymethoxy flavonoid, exerts anti-allergic effect by suppressing activation of phosphoinositide 3-kinase,* Journal of Functional Foods, 6, 606-614, 2014.

[8] Young, D.A. and Sterner, R.W., *Leaf flavonoids of primitive dicotyledonous angiosperms: Degeneria vitiensis and Idiospermum australiense,* Biochemical Systematics and Ecology, 9 (2), 185-187, 1981.

[9] Truchado, P., Ferreres, F., and Tomas-Barberan, F.A., *Liquid chromatography-tandem mass spectrometry reveals the widespread occurrence of flavonoid glycosides in honey, and their potential as floral origin markers,* Journal of Chromatography. A, 1216 (43), 7241-8, 2009.

[10] Solgun, D.G., Tanriverdi, A.A., Yildiko, U., and Ağirtaş, M.S., *Synthesis of axially silicon phthalocyanine substituted with bis- (3,4-dimethoxyphenethoxy) groups, DFT and molecular docking studies,* Journal of Inclusion Phenomena and Macrocyclic Chemistry, 102 (11), 851-860, 2022.

[11] Cui, W., Chen, J., *Insight into mineral flotation fundamentals through the DFT method,* International Journal of Mining Science and Technology, 31 (6), 983-994, 2021.

[12] Chauhan, A., Singh, K.M., *Recursive sliding DFT algorithms: A review,* Digital Signal Processing, 127, 103560, 2022.

[13] Shang, Y., Duan, X., Wang, S., Yue, Q., Gao, B., and Xu, X., *Carbon-based single atom catalyst: Synthesis, characterization, DFT calculations,* Chinese Chemical Letters, 33 (2), 663-673, 2022.

[14] Frisch, M.J., Trucks, G.W., Schlegel, H.B., and Scuseria, G.E., Gaussian 09, Revision E.01, 2016.

[15] Wang, G., Liu, W., Gong, Z., Huang, Y., Li, Y., and Peng, Z., *Design, synthesis, biological evaluation and molecular docking studies of new chalcone derivatives containing diaryl ether moiety as potential anticancer agents and tubulin polymerization inhibitors,* Bioorganic Chemistry, 95, 103565, 2020.

[16] Altun, K., Yildiko, Ü., Tanrıverdi, A.A., Tekeş, A.T., Ata, A.Ç., Kartal, B., and Çakmak, İ., *Structural and Spectral Properties of 4-(5-methyl-[1, 2, 4] triazolo [1, 5-a] pyrimidine-7-yloxy) phthalonitrile: Analysis by TD-DFT Method, ADME Analysis, and Molecular Docking Simulations,* Journal of the Institute of Science Technology, 12 (4), 2340-2351, 2022.

[17] Yildiko, Ü., Türkan, F., Tanriverdi, A.A., Ata, A.C., Atalar, M.N., and Cakmak, İ., *Synthesis, enzymes inhibitory properties and characterization of 2-(bis (4-aminophenyl) methyl) butan-1-ol compound: Quantum simulations, and in-silico molecular docking studies,* Journal of the Indian Chemical Society, 98 (11), 100206, 2021.

[18] Akinpelu, O.I., Lawal, M.M., Kumalo, H.M., and Mhlongo, N.N., *Drug repurposing: Fusidic acid as a potential inhibitor of M. tuberculosis FtsZ polymerization – Insight from DFT calculations, molecular docking and molecular dynamics simulations,* Tuberculosis, 121, 101920, 2020.

[19] Asadi, Z., Golchin, M., Eigner, V., Dusek, M., and Amirghofran, Z., *A detailed study on the interaction of a novel water-soluble glycine bridged zinc(II) Schiff base coordination polymer with BSA: Synthesis, crystal structure, molecular docking and cytotoxicity effect against A549, Jurkat and Raji cell lines,* Inorganica Chimica Acta, 465, 50-60, 2017.

[20] Marinho, E.M., Batista de Andrade Neto, J., Silva, J., Rocha da Silva, C., Cavalcanti, B.C., Marinho, E.S., and Nobre Júnior, H.V., *Virtual screening based on molecular docking of possible inhibitors of Covid-19 main protease,* Microbial Pathogenesis, 148, 104365, 2020.

[21] Solğun, D.G., Keskin, M.S., yıldıko, Ü., and Ağırtaş, M.S., *DFT analysis and electronic properties, and synthesis of tetra (9-phenyl-9H-xanthen-9-yl) oxy peripheral-substituted zinc phthalocyanine,* Chemical Papers, 74 (8), 2389-2401, 2020.

[22] Khajehzadeh, M. and Moghadam, M., *Molecular structure, FT IR, NMR, UV, NBO and HOMO–LUMO of 1-(3-(dimethylamino)propyl)-1-(4-fluorophenyl)-1,3-dihydroisobenzofuran-5-carbonitrile by DFT/B3LYP and PBEPBE methods with LanL2DZ and 6-311++G(d,2p) basis sets,* Spectrochimica Acta Part A: Molecular and Biomolecular Spectroscopy, 180, 51-66, 2017.

[23] Yildiko, Ü., Ata, A.Ç., Tanriverdi, A.A., and Çakmak, İ., *Investigation of novel diethanolamine dithiocarbamate agent for RAFT polymerization: DFT computational study of the oligomer molecules,* Bulletin of Materials Science, 44 (3), 186, 2021.

[24] Li, K., Xu, W., Han, M., Cheng, Y., Wen, G., and Huang, T., *Integration of iron-manganese co-oxide (FMO) with gravity-driven membrane (GDM) for efficient treatment of surface water containing manganese and ammonium,* Separation and Purification Technology, 282, 119977, 2022.

[25] Griesbeck, C., Hager-Braun, C., Rogl, H., and Hauska, G., *Quantitation of P840 reaction center preparations from Chlorobium tepidum: chlorophylls and FMO-protein,* Biochimica et Biophysica Acta (BBA) - Bioenergetics, 1365 (1), 285-293, 1998.

[26] Tanriverdi, A.A., Yildiko, U., Tekes, A.T., Cakmak, İ., and Ata, A.C., *Synthesis, characterization and affinity detection of sulfonated polyimides: confirmation of proton transfer in quantum theory simulations,* Polymer Bulletin, 2022. DOI: https://doi.org/10.1007/s00289-022-04536-0

[27] Tekeş, A.T., Ata, A.Ç., Tanriverdi, A.A., and Çakmak, İ., *Insilico Molecular Docking Studies of THBF Compound: TD-DFT Simulations and Drug Design,* Journal of the Institute of Science Technology, 11 (4), 2955-2966, 2021.

[28] Durgadevi, R., Suvitha, A., and Arumanayagam, T., *Growth, optical, electrical properties and DFT studies on piperidinium 4-nitrophenolate NLO single crystal in acetone,* Journal of Crystal Growth, 582, 126512, 2022.

[29] Derafa, W., Aggoun, D., Messasma, Z., Houchi, S., Bouacida, S., and Ourari, A., *An unexpected single crystal structure of nickel(II) complex: Spectral, DFT, NLO, magnetic and molecular docking studies,* Journal of Molecular Structure, 1264, 133190, 2022.

[30] Al Sabahi, A., Al Busafi, S.N., Suliman, F.O., and Al Kindy, S.M., *Photophysical and theoretical studies on the solvatochromic effects and dipole moments evaluation of substituted 1-phenyl-3-naphthyl-5- (4-ethyl benzoate)-2-pyrazoline,* Journal of Molecular Liquids, 307, 112967, 2020.

[31] Arivazhagan, M. and Senthil kumar, J., *Molecular structure, vibrational spectral assignments, HOMO–LUMO, MESP, Mulliken analysis and thermodynamic properties of 2,6-xylenol and 2,5-dimethyl cyclohexanol based on DFT calculation,* Spectrochimica Acta Part A: Molecular and Biomolecular Spectroscopy, 137, 490-502, 2015.

[32] Priya, M.K., Revathi, B.K., Renuka, V., Sathya, S., and Asirvatham, P.S., *Molecular Structure, Spectroscopic (FT-IR, FT-Raman, 13C and 1H NMR) Analysis, HOMO-LUMO Energies, Mulliken, MEP and Thermal Properties of New Chalcone Derivative by DFT Calculation,* Materials Today: Proceedings, 8, 37-46, 2019.

[33] Akman, M., Ata, A.C., Yildiko, U., and Çakmak, İ., *Molecular structure, frontier molecular orbitals, NBO, MESP and thermodynamic properties of 5,12-dibromo perylene with DFT calculation methods,* International Journal of Chemistry and Technology, 4 (1), 49-59, 2020.

[34] Boshaala, A., Said, M.A., Assirey, E.A., Alborki, Z.S., AlObaid, A.A., Zarrouk, A., and Warad, I., *Crystal structure, MEP/DFT/XRD, thione ⇌ thiol tautomerization, thermal, docking, and optical/TD-DFT studies of (E)-methyl 2-(1-phenylethylidene)-hydrazinecarbodithioate ligand,* Journal of Molecular Structure, 1238, 130461, 2021.

[35] Murugan, P., Jeyavijayan, S., Ramuthai, M., and Narmadha, R.B., *Structural, Spectroscopic, NBO and Molecular Docking Analysis of 5-Nitrobenzimidazole – A DFT Approach,* Polycyclic Aromatic Compounds, 2022. DOI: https://doi.org/10.1080/10406638.2022.2056621